Bio-nanocomposites Based on Compatibilized Poly(Lactic Acid) Blend-reinforced Agave Cellulose Nanocrystals

Noor Afizah Rosli,[a,b,*] Wan Hafizi Wan Ishak,[a] Siti Salwani Darwis,[a] Ishak Ahmad,[a,b,*] and Mohammad Fauzul Azim Mohd Khairudin [a]

Enhancing the mechanical, thermal, and degradation properties of a poly(lactic acid) (PLA) blend without deteriorating its other useful features was the goal of this work. The isolation of cellulose nanocrystals (CNCs) from *Agave angustifolia* fibers was carried out, and the properties of the bio-nanocomposites comprising these CNCs were evaluated, which included PLA, natural rubber (NR), and liquid NR (LNR). Transmission electron microscopy and zeta potential analysis confirmed the successful isolation of CNCs from agave fibers after several chemical treatment steps. The effects of different CNC loadings on the properties of the bio-nanocomposites were investigated using tensile tests, thermal analysis, morphological analysis, and water absorption tests. Bio-nanocomposites containing 5 wt% and 7.5 wt% CNC had the optimal tensile modulus and strength, respectively. Different levels of CNC did not noticeably affect the thermal stability of the bio-nanocomposites, although the thermogram curves increased slightly as CNC content increased. The addition of CNC at different loadings affects the crystallization rate of PLA blend. The water absorption capacity increased as CNC level increased, and 5 wt% CNC gave rise to the highest water absorption. The four-component bio-nanocomposites created in this study provided an alternative for producing new green materials with tunable physical, mechanical, and thermal properties.

Keywords: Biodegradable; Biopolymer; Green composite; Liquid natural rubber

Contact information: a: Department of Chemical Sciences, Faculty of Science and Technology, Universiti Kebangsaan Malaysia, 43600 Bangi, Selangor, Malaysia; b: Polymer Research Center (PORCE), Faculty Science and Technology, Universiti Kebangsaan Malaysia, 43600 Bangi, Selangor, Malaysia;
** Corresponding author: nafizah@ukm.edu.my (N.A. Rosli); gading@ukm.edu.my (Ahmad. I)*

INTRODUCTION

The use of synthetic plastic products in daily life has resulted in enormous plastic waste and unacceptable environmental contamination. Because of this important issue, the use of biodegradable polymers or renewable polymers that are environmentally friendly is being extensively explored. Poly(lactic acid) (PLA) is one such bio-based plastic that has received a lot of attention due to its excellent mechanical properties that are comparable to synthetic plastics, such as polyethylene terephthalate. For example, blending of PLA with natural rubber (NR) has been studied extensively (Jaratrotkamjorn *et al.* 2012; Bijarimi *et al.* 2013; Si *et al.* 2018). The addition of NR improves the toughness, thermal stability, biodegradability, and nucleation properties of PLA, and it preserves its green properties (Bitinis *et al.* 2011; Jaratrotkamjorn *et al.* 2012). However, the PLA/NR blend requires a compatibilizer to enhance the tensile properties and adhesion of the blend (Ock *et al.* 2016;

Pongsathit and Pattamaprom 2018). Liquid NR (LNR) is one such compatibilizer that successfully increases the tensile and other properties of this blend, and it maintains its green features (Rosli *et al.* 2016). LNR has the same microstructure as NR, except it has the additional reactive groups of –OH, -OOH, and C=O at the end of its chains (Abdullah 1994; Rosli *et al.* 2016). LNR can sufficiently cause stress transfer in the composites due to its spherical domains, thus preventing the failure of the material (Mathew *et al.* 2010).

The potential of the PLA/NR-compatibilized LNR blend can be further exploited by introducing new natural reinforcing materials. Cellulose has been used as a reinforcement material in PLA and NR for decades to reduce the cost of the end materials, reduce density, and improve biodegradability as well as a viable route to extend its application while maintaining the "greenness" (Bras *et al.* 2010; Frone *et al.* 2011; Visakh *et al.* 2012). Cellulose is a semi-crystalline polymer comprised of D-glucopyranosyl repeating units that are linked together by hydrogen bonds to form a fibril. Previously, cellulose isolated from the *Agave angustifolia* plant (Fig. 1) has been used as a reinforcement material for PLA/NR compatibilized LNR blends (Rosli *et al.* 2019a). Agave cellulose successfully improves the tensile strength, tensile modulus, thermal stability, and degradability of PLA/NR/LNR biocomposites. Therefore, attempts have been made to further increase the utility of agave cellulose as a reinforcing material using chemical treatments.

Fig. 1. *Agave angustifolia* plants

Agave angustifolia fibers mainly consist of cellulose with a 67% α-cellulose content (Rosli *et al.* 2013), making it a suitable cellulose source. The utility of agave cellulose can be improved by chemical or mechanical treatments that cause its disintegration to produce nano-sized cellulose particles, which are also referred to as nanofibrillated cellulose (NFC) or cellulose nanocrystals (CNCs) (Trache *et al.* 2017; Collazo-Bigliardi *et al.* 2018). It is expected that nanocomposites with CNC reinforcement will exhibit enhanced mechanical strength and biodegradability and reduce the final product weight. A cellulose nanocrystal is an individual crystal that possesses high strength, high crystallinity, a large surface area, and a high aspect ratio. Due to these excellent features, superior interaction can be achieved

between agave CNC and PLA/NR/LNR blended matrices, which enhances the properties of the nanocomposites (Thomas *et al.* 2015; Indarti *et al.* 2016).

A previous study by Bitinis *et al*. (2013) reported the use of CNC extracted from commercial microcrystalline cellulose in a PLA/NR blend. However, the study only examined the use of 3 wt% CNC in PLA/NR nanocomposites, and the effect of LNR as a compatibilizer in PLA/NR reinforced with CNC nanocomposite was not explored. This study aimed to investigate the use of CNC isolated from *Agave angustifolia* in the fabrication of PLA/NR-compatibilized LNR-based nanocomposites. Various agave CNC contents were incorporated into the PLA blend, and the mechanical, thermal, and water absorption features of the resulting bio-nanocomposites were assessed.

EXPERIMENTAL

Materials

Poly(lactic acid) grade 2003D and NR grade SMR-L were purchased from NatureWorks (Minnetonka, Minnesota, USA) and the Malaysian Rubber Board (Petaling Jaya, Malaysia), respectively. The chemical reagents used for the preparation of LNR, such as toluene, rose Bengal, and methylene blue were purchased from Sigma-Aldrich (St. Louis, Missouri, USA), and methanol was purchased from Classic Chemicals Sdn. Bhd. (Shah Alam, Malaysia). *Agave angustifolia* leaves were collected from Selangor, Malaysia. Materials used in the extraction of CNCs, such as sodium chlorite ($NaClO_2$) and glacial acetic acid (99%), were purchased from Sigma-Aldrich (St. Louis, Missouri, USA), sulfuric acid (H_2SO_4, 98%) was purchased from Univar Solutions (Downers Grove, Illinois, USA), and sodium hydroxide (NaOH) was purchased from Classic Chemicals Sdn. Bhd. (Shah Alam, Malaysia).

Synthesis of LNRs

The preparation of LNRs has been previously described (Abdullah 1994; Rosli *et al.* 2016). Natural rubber was swelled in toluene for 24 h. After it had expanded entirely, it was mechanically stirred at 80 °C. The process was conducted under visible light and was deemed complete after the dye was completely invisible in the irradiation medium. After irradiation in toluene medium was complete, the NR became LNR viscous liquid. To obtain LNR in liquid form, the gel portion of LNR was separated through centrifugation at 5,000 rpm for 5 min.

Isolation of CNCs

The CNCs were isolated from the agave fibers as previously described (Sheltami *et al.* 2012). The long fibers were retted in water for 4 d until the green color turned white. Following this, the fibers were cut into pieces 5 cm long, ground with a grinder, and sieved at a range from 250 µm to 500 µm. The fibers were then treated with alkali by incubating them for 2 h at 80 °C to 100 °C in 4% NaOH. Then, they were bleached for 4 h with 1.7 w/v% $NaClO_2$ at 80 °C to 100°C. The alkali and bleaching treatments were repeated twice, and after each treatment, the fibers were washed with distilled water. Subsequently, the bleached agave fibers were subjected to acid hydrolysis by stirring them for 30 min at 45 °C in 60 wt% H_2SO_4. The hydrolysis reaction was stopped by the addition of ice cubes to the hydrolyzed cellulose. Next, the hydrolyzed cellulose was washed several times, and it

was then centrifuged at 10,000 rpm for 5 min after each washing cycle. Finally, the hydrolyzed CNCs were dialyzed against distilled water until they reached a neutral pH.

Preparation of Bio-nanocomposites

Cellulose nanocrystals were obtained from toluene solvent with the solvent exchange technique. Toluene was mixed with the CNC suspension in a centrifuge tube, and the CNCs were pelleted by centrifugation at 5,000 rpm for 5 min. This process was repeated three times, after which all of the water had been removed from the tubes. The CNCs in toluene were prepared at a variety of concentrations (2.5 wt%, 5 wt%, 7.5 wt%, and 10 wt%), mixed with LNR, and briefly sonicated. Melt compounding of the nanocomposites was conducted at 175 °C using a Haake Rheocord internal mixer (Thermo Fisher Scientific, Waltham, MA, USA). First, the premixed CNCs in LNR were allowed to stand in the mixer for 2 min, after which the NR was added, and the rotor was rotated at 60 rpm. Finally, the PLA was added and further mixed for 5 min. Lastly, the nanocomposite was pelletized, dried, and molded using a LABTECH LP 50 (Labtech Engineering Company Ltd., Samutprakarn, Thailand) hydraulic press. The pelletized sample was initially hot compressed for 10 min at 175 °C and then immediately cold compressed for 15 min.

Characterization

A Philips CM12 (Hillsboro, OR, USA) transmission electron microscope (TEM) was used to determine the dimensions and morphology of the agave CNCs. The suspension of CNCs was diluted and dropped onto the surface of a copper grid covered with a thin carbon film. The surface of the copper grid was stained with 2 wt% uranyl acetate after the excess water on the copper grid surface was removed using filter paper. The stained copper grid was air-dried, and the sample was observed using an accelerating voltage of 80 kV.

A Litesizer 500 device was used to investigate the zeta potential of CNC in neutral water. Calculation based on the electrophoretic mobility of the suspension was used, where it was converted to zeta potential.

The glass transition temperature (T_g), crystallization temperature (T_c), and melting temperature (T_m) of the bio-nanocomposites were determined by differential scanning calorimetry (DSC) analysis using the Mettler Toledo DSC 882e. Samples were weighed and heated at room temperature to 200 °C at a heating rate of 10 °Cmin^{-1} with a nitrogen gas flow rate of 10 mLmin^{-1}.

Thermogravimetric analysis (TGA) was conducted on the CNC and the bio-nanocomposite samples. The homogenized CNC suspension was frozen in a freezer and then freeze-dried to produce a solid CNC form. The CNC in solid form and the bio-nanocomposites were weighed and subjected to TGA analysis using a Mettler Toledo (Columbus, OH, USA) thermogravimetric analyzer (TGA/SDTA851e). All the samples were placed in an aluminum pan and tested from room temperature up to 600 °C. The analysis was done under a nitrogen gas environment with a heating rate of 10 °C min^{-1}.

The tensile test for the PLA/NR/LNR/CNC nanocomposites was performed at 16 °C. The PLA/NR/LNR/CNC bio-nanocomposites were first cut to have dimensions of 70 mm × 15 mm × 3 mm in length, width, and thickness, respectively. A universal testing machine model 5566 (Instron, Norwood, MA, USA) was used to perform the tensile test at standard test parameters: a gauge length of 40 mm, a cross-head speed of 10 mm/min, and a load cell of 10 kN. The tensile property values were reported as the average of five tested samples.

The bio-nanocomposite and blend samples were cryogenically fractured using liquid nitrogen. Then, the sample was dried in an oven and coated with platinum to prevent charge accumulation on the sample surface. The morphology of the sample's fractured surface was viewed using field emission scanning electron microscopy (FESEM) model Zeiss Supra 55VP at accelerating voltage of 3 kV and magnification of 1000 x.

The ability of the PLA/NR/LNR/CNC bio-nanocomposites to absorb water was investigated following the ASTM D570 (1998) standard method (Rosli *et al.* 2019a). The dried samples were weighed and immersed in distilled water at 24 °C. The sample was patted dry and weighed at 1-day intervals. The ability of the PLA/NR/LNR/CNC nanocomposites to absorb water was expressed as shown in Eq. 1,

$$\% \text{ of Water absorption} = (w_o - w_o) / w_o \times 100 \quad (1)$$

where w_i and w_o are the wet and dry weights of the sample (5 units), respectively. Cellulose nanocrystals in toluene solvent were obtained through the solvent exchange technique. Toluene was mixed with the CNC suspension in a centrifuge tube, and the CNCs were pelleted by centrifugation at 5,000 rpm for 5 min. This process was done a total of 3 cycles.

RESULTS AND DISCUSSION

CNC Characterization

Typically, H_2SO_4 treatment is used to produce CNCs from cellulose (bleached fibers). The amorphous domain of cellulose can be removed by cleaving the microfibrils under the appropriate acid hydrolysis conditions. The cleaving of the cellulose microfibrils also keeps the crystalline domains intact. Furthermore, it helps to disintegrate and defibrillate the cellulose microfibrils. As a result, CNCs with nanometer dimensions and high stability in water were produced (Fig. 2). The stable aqueous suspension obtained was mainly due to the charged surface of the crystalline domain gained through the H_2SO_4 treatment. The charges between the CNC nanoparticles then induce electrostatic repulsion forces resulting in a stable CNC suspension (Samir *et al.* 2004; Zainuddin *et al.* 2017). The yield of cellulose extracted by this method is 97%. Alkali and bleaching treatments significantly yield a higher amount of cellulose, since the treatment successfully eliminated most hemicellulose and lignin content (Rosli *et al.* 2013). Other methods such as organosolv and soda methods used to extract cellulose from *Agave tequilana* yields 67% and 56 % cellulose, respectively (Hernández *et al.* 2018).

Figure 2b confirms the success of the H_2SO_4 treatment of agave cellulose, as it is shown to have been separated to form individual nanoparticles. The lengths (*l*), widths (*d*), and aspect ratios (l/*d*) of 50 individual CNC particles are shown in Table 1. The length of the agave CNCs ranged from 100 nm to 400 nm, with an average value of approximately 200 nm. Table 1 shows that the diameter and the aspect ratio of agave CNCs ranged from 10 nm to 25 nm and 10 to 15, respectively. Similar values were reported by Johar *et al.* (2012) using CNCs isolated from rice husk fibers. A detailed morphology and properties of fibers after different stages of preparation have been reported previously (Rosli *et al.* 2013). Upon each treatment, the diameter of the fibers reduced significantly, as well as the surface of the fibers become smoother. As for crystalline properties, CNCs show 82.4% of crystallinity index after hydrolysis treatments (Rosli *et al.* 2013).

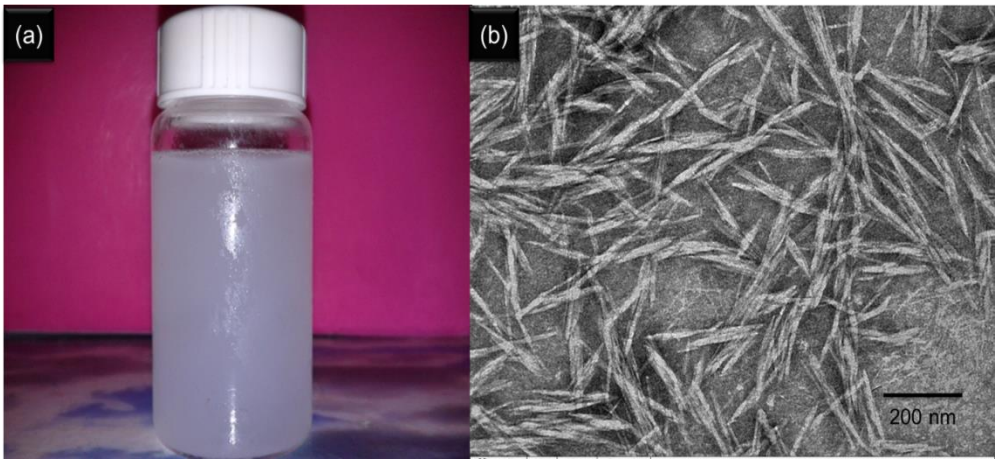

Fig. 2. (a) Photograph of the agave CNC suspension and (b) TEM micrograph of agave CNCs

Table 1. Properties of *Agave angustifolia* CNC

Properties of CNC	Diameter (nm)	Aspect ratio (l/d)	Length (nm)	Zeta potential (mV)
	10 to 25	10 t0 15	100 to 400	-33.4

The electrokinetic character governing the stability of a CNC dispersion in an aqueous medium was studied using zeta potential measurements. The CNC suspension in neutral water showed a negative value of zeta potential at -33.4 mV, as shown in Fig. 3. The negative value is due to the presence of a large number of negatively charged sulfate groups on the surface of CNC and the increase in the surface charge of the particles (Kargarzadeh *et al*. 2012). These effects are the main reasons for the high dispersion stability in CNCs obtained from the H_2SO_4 hydrolysis method.

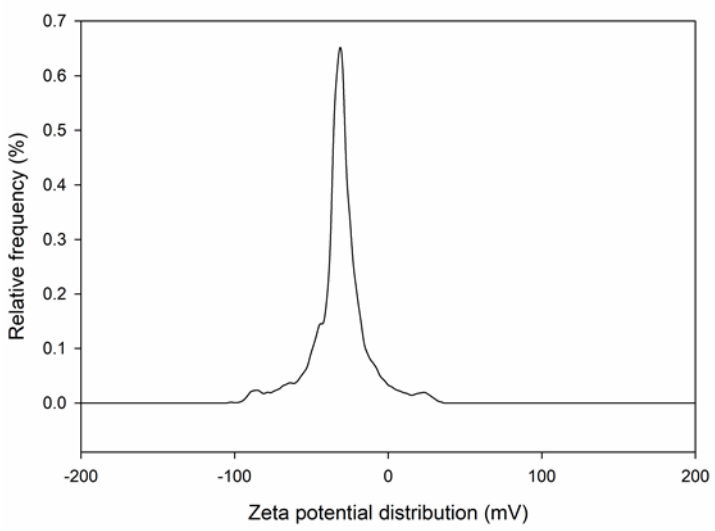

Fig. 3. Zeta potential distribution of agave CNC

The thermogravimetric analysis determined the suitability of the agave CNCs for use in high-temperature applications. Figure 4 shows the thermal stability properties of the agave CNCs over a temperature range of 35 to 600 °C. The TG curves showed a three-

stage degradation process for the agave CNC, and the first step was related to the evaporation of moisture absorbed by the CNCs. The weight loss measured at 165 to 285 °C in the second stage was associated with the decomposition of sulfated regions. The amorphous part of the sulfated group made it highly accessible, which resulted in tremendous weight loss at low temperatures.

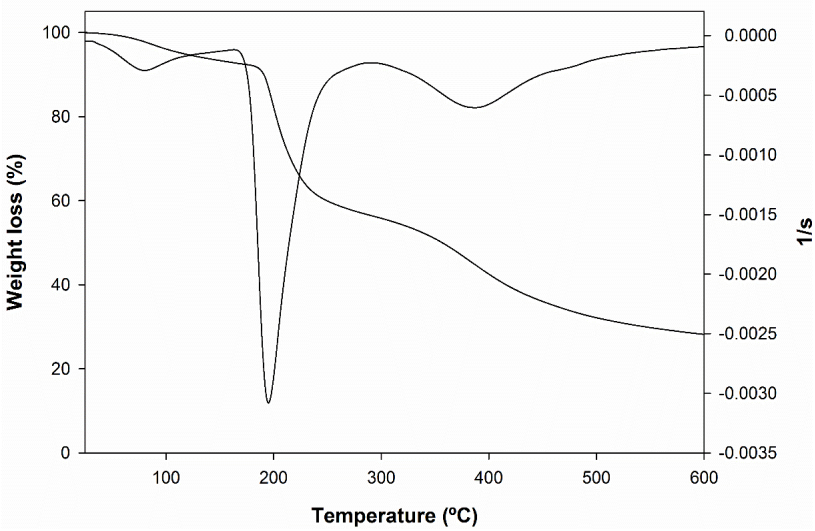

Fig. 4. The TGA and derivative thermogravimetric (DTG) thermograms of agave CNCs

The last degradation step occurred at 300 to 460 °C and was attributed to the decomposition of unsulfated crystals (De Morais Teixeira *et al.* 2011). Previously, it has been reported that agave cellulose starts to degrade at 260 to 398 °C (Rosli *et al.* 2013). Many factors can affect the low stability of agave CNCs, such as the presence of sulfate groups and the dimensions of the CNCs. The presence of sulfate groups causes a dehydration reaction to occur, and the negative charge on the outer surface of the CNCs directly reduces the thermal stability of the CNCs (Roman and Winter 2004; Fahma *et al.* 2010; Kassab *et al.* 2019). Concerning dimensions, the small nano-scale and crystallite size caused a reduction in thermal stability by increasing the aspect ratio and surface area of the CNCs. The high surface areas increased heat exposure and partially disrupted the crystal structure of cellulose (Liu *et al.* 2016). Furthermore, the presence of sulfate groups resulted in high residue content (> 20 wt%) for agave CNCs at 600 °C, at which temperature the sulfate acts as a flame retardant and causes char formation (Roman and Winter 2004).

Tensile Properties of the Bio-nanocomposites

The evaluation of the tensile strength as a function of CNC loading and stress-strain curves of PLA/NR/LNR bio-nanocomposites are shown in Figs. 5 and 6, respectively. As indicated, the addition of 2.5 wt% CNCs caused a slight decrease in the tensile strength, whereas the addition of 7.5 wt% CNCs increased the tensile strength of the nanocomposite. However, the tensile strength decreased beyond the optimum loading. At low CNC loading (2.5 wt%), the CNC insufficiently reinforced the PLA/NR/LNR blend due to a high-stress concentration. This causes a phenomenon called the dilution effect, in which bond breakage occurs between the CNC and the PLA/NR/LNR blend (De and White 1996; Rosli *et al.* 2016). Kargarzadeh *et al.* (2015) reported a similar phenomenon with the addition of a low kenaf CNC content in the polyester/liquid epoxidized NR blend. In addition, this

phenomenon was also observed in cellulose reinforced NR, PLA, and PLA/NR/LNR biocomposites (Ismail *et al.* 2003; Shah *et al.* 2008; Rosli *et al.* 2016). Interestingly, agave CNCs showed a good ability to maintain the tensile strength of the PLA/NR/LNR blend at low fiber contents compared with previous studies using agave cellulose (Rosli *et al.* 2016). A slight decrement of about 1.2% was noticed with the incorporation of 2.5 wt% agave CNC, and the tensile strength was remarkably reduced up to 12.5% with the addition of 2.5 wt% agave cellulose.

The improvement of the agave CNC reinforced PLA/NR/LNRs up to 4 and 11% at loadings of 5 wt% and 7.5 wt% CNC was attributed to the high aspect ratios and surface areas of the CNCs. A high surface area results in effective stress transfer between CNCs and the PLA/NR/LNR blend, which increases the tensile strength (Fu *et al.* 2008). This led to better reinforcement of CNCs in the PLA/NR/LNR blend. Another reason for the high tensile strength was the good interfacial adhesion between the CNCs and the PLA/NR/LNR blend due to a chemical interaction between the CNCs and the PLA and LNR matrix. The study of Rosli *et al*. (2019a) has demonstrated the interaction between *Agave angustifolia* cellulose with PLA and LNR. Owing to similar FTIR spectra of *Agave angustifolia* CNC and cellulose, it can be concluded that similar interactions occur between CNC with PLA and LNR. Chemical interactions occur between hydroxyl groups of cellulose with hydroxyl and carbonyl groups of PLA. In addition, chemical interactions also occur between the hydroxyl group of cellulose with the carbonyl group of LNR (Rosli *et al.* 2019a). To get a clearer picture, Fig. 7 shows a schematic diagram of the interface between the components in a bio-nanocomposite. An improvement in tensile strength following the incorporation of CNCs into a starch matrix was reported by Kargarzadeh *et al.* (2017), who found that CNCs had a good interaction with starch, and CNC networks formed within the nanocomposite films.

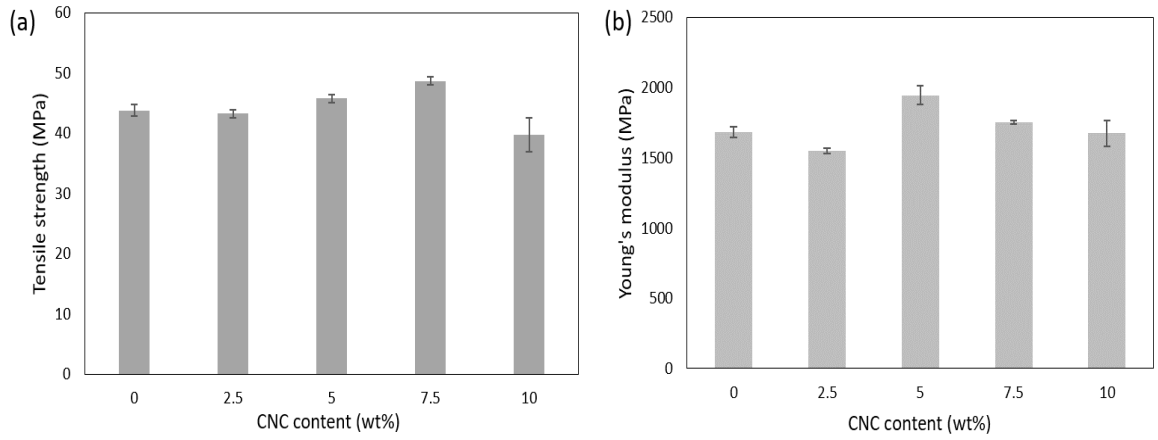

Fig. 5. Tensile strength of PLA/NR/LNR/CNC bio-nanocomposites

However, the tensile strength of the PLA/NR/LNR/CNC nanocomposite decreased with the addition of CNCs beyond the optimum level. The three-dimensional network formed by the intra- and intermolecular hydrogen bonds between CNCs may have also negatively affected the tensile strength of the nanocomposite. The three-dimensional CNC network may have caused the formation of CNC agglomerates in the system, which likely resulted in the non-homogeneous dispersion of the CNCs. Furthermore, the decrease of tensile strength at this loading was likely due to the aggregation of CNCs in the matrix

phase. Because the aggregation and agglomeration of CNCs hindered the fiber dispersion, the efficiency of stress transfer from the CNCs to PLA/NR/LNR blend also suffered, which reduced the tensile strength.

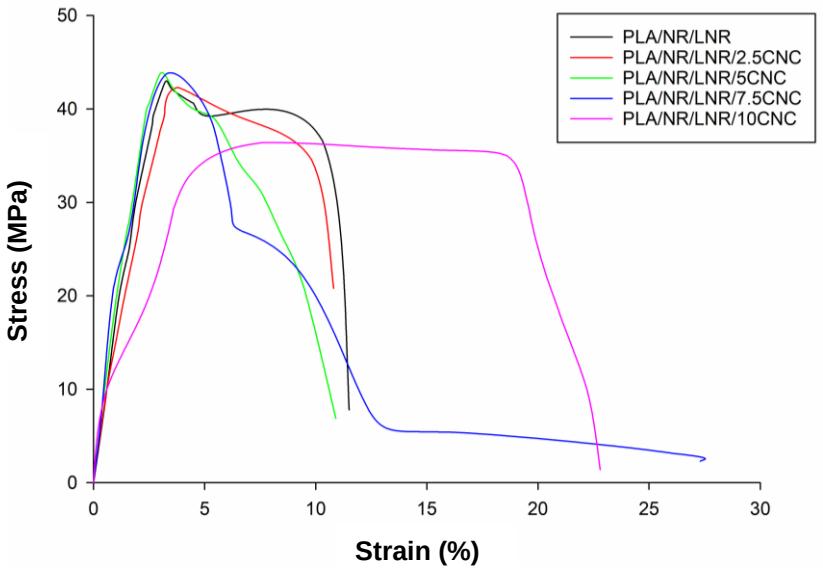

Fig. 6. Stress-strain curves of PLA/NR/LNR blend and bio-nanocomposites

The Young's moduli of different PLA/NR/LNR/CNC nanocomposites are shown in Fig. 5(b). A slightly similar trend to that of tensile strength was observed for Young's modulus, which decreased with the addition of 2.5 wt% CNCs, gradually increased up to 5 wt% CNC, and then dropped at 7.5 wt% CNC loading. However, Young's modulus value recorded for the PLA/NR/LNR/7.5 wt% CNC bio-nanocomposite was still higher than that of the PLA/NR/LNR blend alone. Again, the dilution effect of the matrix and the aggregation and agglomeration of CNCs negatively impacted both tensile strength and Young's modulus. The increase in Young's modulus was likely due to the highly crystalline nature of the CNCs, which increased the stiffness of the nanocomposites. As stiffness increases, the dissipation energy from the PLA/NR/LNR blend matrix also decreases, which increases Young's modulus (Tronc *et al.* 2007).

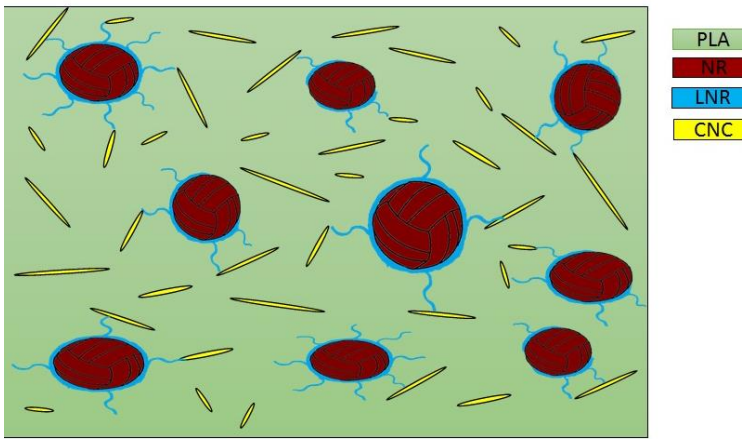

Fig. 7. Schematic diagram of the interface of the bio-nanocomposite

One-way ANOVA analysis of tensile properties data of different CNC loading with a significant level of 0.05 is shown in Table 2. The p-value below 0.05, indicated by all three tensile properties, shows that the statistical difference between data was significant with a 95% confidence level. In addition to the p-value, the high F value than F critical also indicates that the effect of CNC addition on changes in tensile properties was significant (Chen *et al*. 2019).

Table 2. One-way ANOVA Test on the Effect of CNC Loading on Tensile Properties

Tensile properties	p-value	F-value	F-critical
Tensile strength	0.011	10.865	5.192
Young' modulus	0.006	14.499	5.192
Elongation at break	0.019	8.472	5.192

Morphological Properties

The morphology of the cryo-fractured surface of the PLA/NR/LNR blends and bio-nanocomposites is shown in Fig. 8. The micrograph in Fig. 8(a) shows that the fractured surface of the PLA/NR/LNR blend exhibited a smoother surface structure than other micrographs. Phase separation of PLA/NR blend resulted in the loss of NR droplets on the surface of the fractured matrix. The addition of CNC caused a change in the NR droplet size, as shown in Fig. 8(b – d). Nevertheless, the distribution of NR droplets on the surface of all bio-nanocomposites was almost the same as the blend.

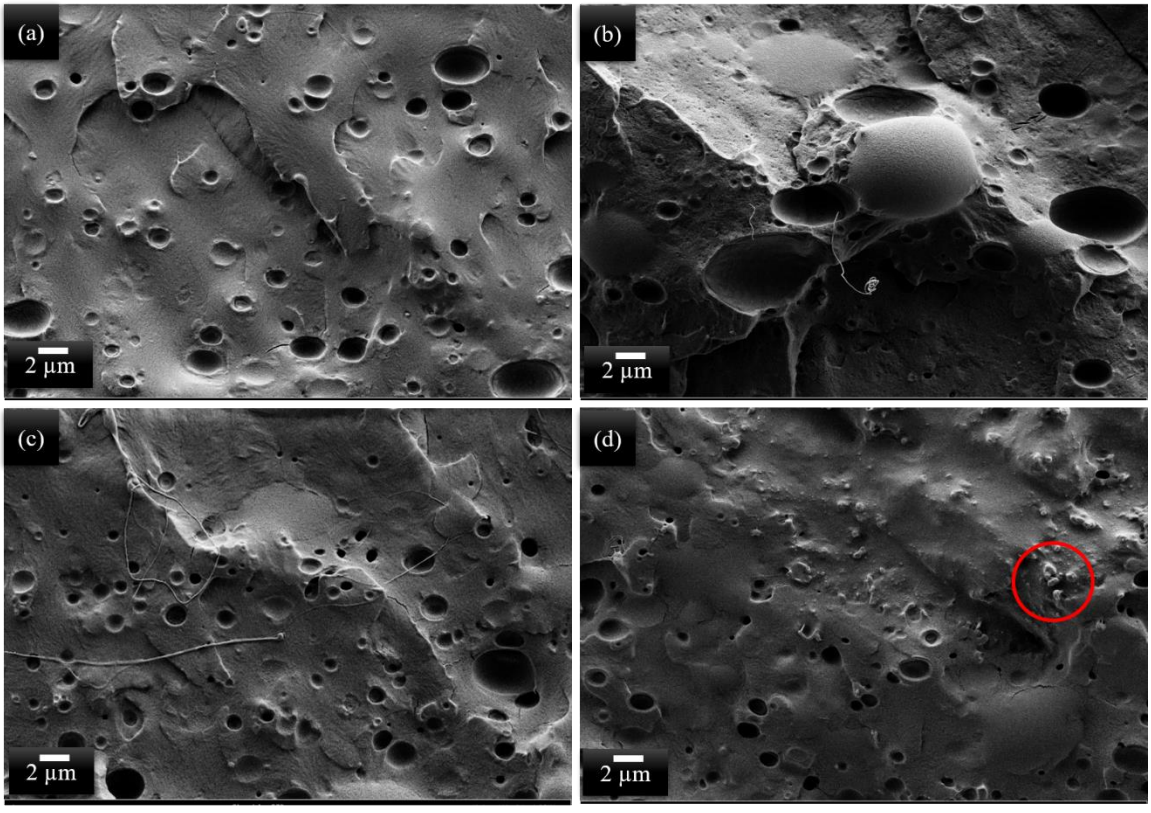

Fig. 8. FESEM micrographs of the cryogenically fractured surface of (a) PLA/NR/LNR blend, (b) PLA/NR/LNR/2.5CNC, (c) PLA/NR/LNR/7.5CNC, and (d) PLA/NR/LNR/10CNC

The minimum size of NR droplets for all samples was the same at 0.2 µm. In comparison, the maximum size of NR droplets on the blend increased from 4.7 µm to 11.3, 8, and 8 µm representing bio-nanocomposites with additions of 2.5, 7.5, and 10 wt%, respectively. According to Bitinis *et al.* (2013), the affinity between CNC and PLA phase is higher than NR due to the polarity of the CNC, which ultimately causes a change in the NR droplet sizes. The dilution effect at the low CNC addition (2.5 wt%) also contributed to the large NR droplet size in this bio-nanocomposite loading. The large NR droplet size at this CNC loading (2.5 wt%) resulted in decreased tensile properties, as discussed in the previous section. The morphological analysis also revealed the agglomeration of CNC that occurred with the addition of 10 wt% of CNC, as circled in Fig. 8(d). Meanwhile, the increase in tensile properties of bio-nanocomposite at 7.5 wt% CNC may have been due to the good interface, as shown in Fig. 8(c). The micrograph of 7.5 wt% CNC bio-nanocomposite showed a morphology similar to that of the PLA/NR/LNR blend, but with the addition of a web-like structure on the surface of the fractured sample. This may refer to the good interaction between CNC with PLA and LNR on this composition.

Thermal Properties of Bio-nanocomposites

Figure 9 shows the DSC curves for PLA/NR/LNR bio-nanocomposites with detailed data mentioned in Table 3. It can be observed that the addition of CNC had a significant effect on the T_g value of PLA in PLA/NR/LNR blends. T_g of PLA slightly decreased with 2.5 wt% CNC and increased with the subsequent addition of CNC, with the maximum value recorded by bio-nanocomposites at 5 wt% CNC. The T_g values showed a similar trend to Young's modulus described in the previous section. In addition, the addition of CNC also had a significant effect on the T_c of PLA in PLA/NR/LNR blends. The addition of CNC affected the T_c, where it decreased with 2.5 wt% CNC and was not visible at the addition of 5 and 7.5 wt% of CNC. Low T_c refers to the low ability of PLA to crystallize and produce a less perfect crystal structure (Zhang *et al.* 2013). However, the T_c reappeared with the addition of 10 wt% CNC. Next, the value of the first T_m at the lower temperature refers to the rearrangement of the crystal during heating due to the nucleation effect, whereas the second T_m represents the melting point of PLA.

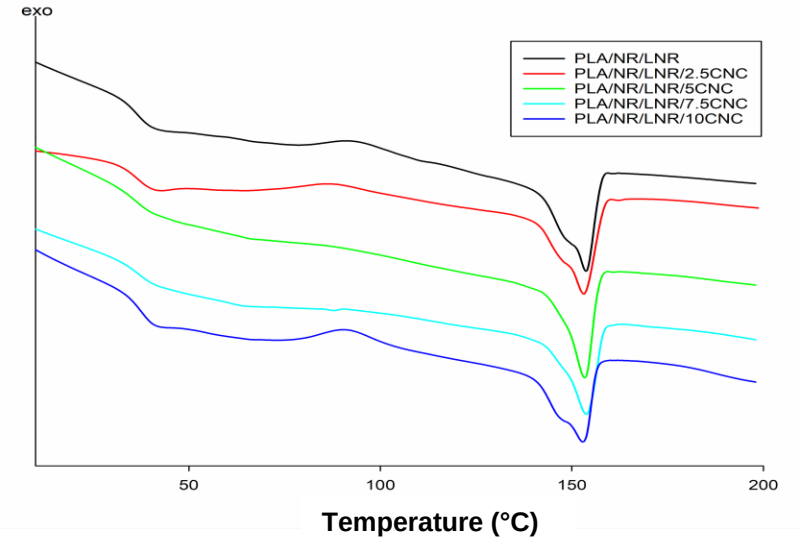

Fig. 9. DSC thermogram of PLA/NR/LNR bio-nanocomposite

Table 3. DSC Data for the Bio-nanocomposites of PLA/NR/LNR/CNC

Samples	T_g (°C)	T_c (°C)	T_{m1} (°C)	T_{m2} (°C)
PLA/NR/LNR	36.9	80.3	148.1	153.4
PLA/NR/LNR/2.5CNC	35.7	72.9	148.1	153.2
PLA/NR/LNR/5CNC	42.0	-	-	153.1
PLA/NR/LNR/7.5CNC	37.9	-	-	152.6
PLA/NR/LNR/10CNC	37.8	78.0	147.1	152.6

Thermal stability properties of the different PLA/NR/LNR/CNC nanocomposites are shown in Fig. 10. The thermograms of the PLA/NR/LNR blend and the different bio-nanocomposites both showed a single-stage decomposition. The PLA/NR/LNR/CNC bio-nanocomposites showed slightly higher thermal degradability than the PLA/NR/LNR blend alone. In addition, the thermal stability of the PLA/NR/LNR/CNC bio-nanocomposites gradually increased as CNC loading increased. The initial degradation at temperatures from 255 to 445 °C was attributed to the degradation of the PLA, NR, and LNR matrices. The maximum degradation temperature of the PLA/NR/LNR blend shifted to a higher temperature (from 355 to 362 °C) with the incorporation of the agave CNCs.

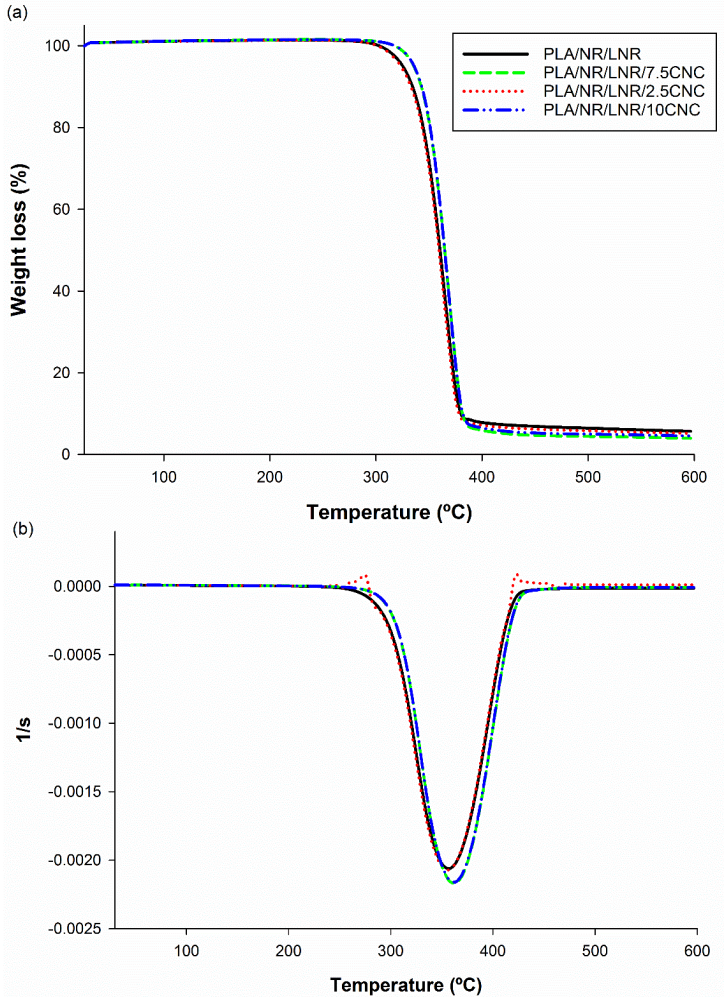

Fig. 10. (a) TGA and (b) DTG curves of the different PLA/NR/LNR/CNC bio-nanocomposites

Generally, the presence of the acidic sulfate group in the H_2SO_4-hydrolyzed CNCs decreases the overall thermal degradability of nanocomposites (Bras *et al.* 2010; Fortunati *et al.* 2013; Khoshkava and Kamal 2014). Previously, it was reported that the thermal stability of PLA improves by up to 2.3 °C with the incorporation of 1 wt% of CNC, but this is accompanied by a reduction in the maximum degradation rate from 2.66%/°C to 1.99%/°C (Lizundia *et al.* 2015). It has also been reported that the incorporation of 10 wt% CNCs decreases the thermal stability of NR from 380 °C to 265 °C (Mariano *et al.* 2016). In this case, the increase in the initial decomposition temperature of the PLA/NR/LNR/CNC bio-nanocomposites could have been due to chemical interactions between the CNCs and PLA and LNR. It has been shown through attenuated total reflectance (ATR)-Fourier transform infrared analysis that chemical interaction between cellulose and PLA and LNR occurs *via* hydrogen bonding (Rosli *et al.* 2016).

Water Absorption of Bio-nanocomposites

Water absorption properties and biodegradability are essential factors in the practical application of newly fabricated biomaterials (Fortunati *et al.* 2012). The biodegradability of PLA is dependent on its water absorption properties, as PLA degradation occurs *via* a hydrolytic process (Rosli *et al.* 2018; Wan Ishak *et al.* 2020). In addition, water facilitates the entry of microorganisms into the system. The presence of microorganisms further increases the biodegradability because the matrix is consumed as a carbon source for the growth of microorganisms. However, water resistance is also essential, especially for uses such as packaging. Therefore, the water absorption percentages of the PLA/NR/LNR/CNC bio-nanocomposites were investigated, and the results are presented in Fig. 11.

As expected, the water absorption percentages of the blend and those of the different bio-nanocomposites of PLA/NR/LNR exhibited similar patterns. Initially, the water absorption increased rapidly, after which it slowed down to reach a plateau at approximately 11 d. The presence of CNCs increased the water absorption percentage of the different PLA/NR/LNR bio-nanocomposites. This behavior was more evident following the addition of 5 wt% CNC, and it was likely due to an increase in the hydrophilicity of the PLA/NR/LNR/CNC bio-nanocomposites, as CNCs could form a three-dimensional network throughout them *via* hydrogen bonding. This phenomenon may influence the water absorption capacity of the bio-nanocomposites (Hossain *et al.* 2012). In addition, the OH groups in the CNCs can react with the –OH groups in the PLA, LNR, and water, which increases the absorption capacity of the PLA/NR/LNR nanocomposites.

However, the water absorption capacity of the nanocomposites gradually decreased with CNC loading greater than 5 wt%, but it was still higher than that of the blend alone. This lower water absorption occurred due to an increase in crystalline regions in the bio-nanocomposites. At low CNC content levels, increased hydrophilicity dominated over the crystallinity effect, which increased water absorption capacity. However, at higher CNC loadings, the crystallinity effect dominated over the hydrophilicity effect, which reduced the water absorption capacity. The highly crystalline, tightly packed nature of CNCs reduced the absorption of water, as the water molecules could not easily penetrate and react with the –OH groups in the CNCs. Based on these water absorption data and previous reports (Rosli *et al.* 2016, 2019b), the fabricated PLA/NR/LNR/CNC bio-nanocomposites have better biodegradability than that of the blend alone.

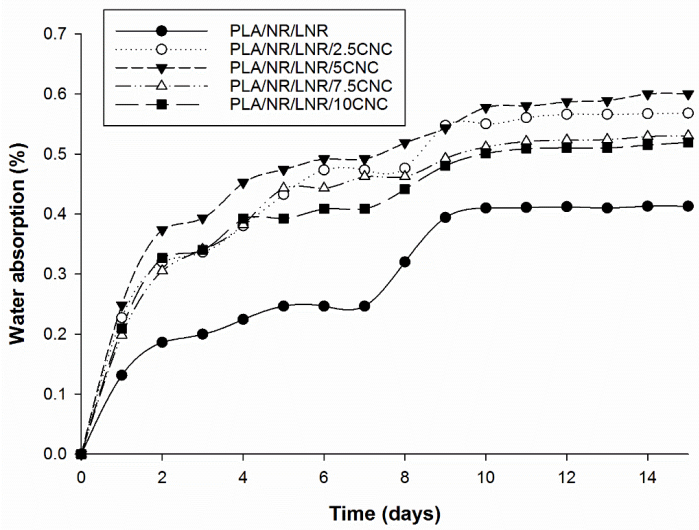

Fig. 11. Water absorption of the different PLA/NR/LNR/CNC nanocomposites

CONCLUSIONS

1. The isolation of cellulose nanocrystals (CNCs) from *Agave angustifolia* fibers was successfully achieved using a series of chemical treatments. The CNCs that were isolated as a result of this procedure had a needle-like structure with an average diameter of 10 to 15 nm.
2. The agave CNCs were successfully used as a reinforcing agent for the poly(lactic acid)/natural rubber/liquid natural rubber (PLA/NR/LNR) nanocomposites. This study demonstrated that the agave CNCs improved the tensile, thermal stability, and water absorption properties of the PLA/NR/LNR bio-nanocomposites.
3. The incorporation of agave CNCs at loadings of 5 wt% and 7.5 wt% into the PLA/NR/LNR blend *via* a melt blending method resulted in bio-nanocomposites with improved tensile properties. The improvement in tensile properties at these fiber loadings was mainly due to the particle size and aspect ratio of the CNCs and the occurrence of hydrogen bonds between the CNCs and PLA and LNR.
4. The addition of CNCs improved the water absorption capability, which could enhanced degradability. The green bio-nanocomposites prepared using agave CNCs, therefore, had improved tensile, thermal stability, and biodegradability properties.

ACKNOWLEDGMENTS

This research was funded by the Ministry of Higher Education of Malaysia (MOHE) (Grant No. MYPAIR/1/2020/TK05/UKM//1) and Universiti Kebangsaan Malaysia (UKM) (Grant No. GUP-2020-048). The authors would like to thank Dr. Md. Akhir Hamid from the Malaysian Agriculture Research & Development Institute (MARDI) for assistance with the extraction of raw fibres from agave leaves.

REFERENCES CITED

Abdullah, I. (1994). "Liquid natural rubber: Preparation and application," *Progress in Pacific Polymer Sciences* 3, 351-365. DOI: 10.1007/978-3-642-78759-1_30

ASTM D570 (1998). "Standard test method for water absorption of plastics," American Society for Testing and Materials, Pennsylvania, United States.

Bijarimi, M., Ahmad, S., and Rasid, R. (2013). "Mechanical, thermal and morphological properties of poly(lactic acid)/natural rubber nanocomposites," *J. Reinf. Plast. Comp.* 32(21), 1656-1667. DOI: 10.1177/0731684413496487

Bitinis, N., Verdejo, R., Cassagnau, P., and Lopez-Manchado, M. A. (2011). "Structure and properties of polylactide/natural rubber blends," *Mater. Chem. Phys.* 129(3), 823-831. DOI: 10.1016/j.matchemphys.2011.05.016

Bitinis, N., Verdejo, R., Bras, J., Fortunati, E., Kenny, J. M., Torre, L., and López-Manchado, M. A. (2013). "Poly(lactic acid)/natural rubber/cellulose nanocrystal bionanocomposites Part I. Processing and morphology," *Carbohyd. Polym.* 96(2), 611-620. DOI: 10.1016/j.carbpol.2013.02.068

Bitinis, N., Fortunati, E., Verdejo, R., Bras, J., Kenny, J. M., Torre, L., and López-Manchado, M. A. (2013). "Poly(lactic acid)/natural rubber/cellulose nanocrystal bionanocomposites. Part II: Properties evaluation," *Carbohyd. Polym.* 96(2), 621-627. DOI: 10.1016/j.carbpol.2013.03.091

Bras, J., Hassan, M. L., Bruzesse, C., Hassan, E. A., El-Wakil, N. A., and Dufresne, A. (2010). "Mechanical, barrier, and biodegradability properties of bagasse cellulose whiskers reinforced natural rubber nanocomposites," *Ind. Crop. Prod.* 32(3), 627-633. DOI: 10.1016/j.indcrop.2010.07.018

Chen, R. S., Amran, N. A. M., and Ahmad, S. (2019). "Reinforcement effect on nano-composites with single/hybrid graphene nanoplatelets and magnesium hydroxide," *J. Therm. Anal. Calorim.* 137(1), 79-92. DOI: 10.1007/s10973-018-7935-y

Collazo-Bigliardi, S., Ortega-Toro, R., and Boix, A. C. (2018). "Isolation and characterization of microcrystalline cellulose and cellulose nanocrystals from coffee husk and comparative study with rice husk," *Carbohyd. Polym.* 191, 205-215. DOI: 10.1016/j.carbpol.2018.03.022

De Morais Teixeira, E., Bondancia, T. J., Teodoro, K. B. R., Corrêa, A. C., Marconcini, J. M., and Mattoso, L. H. C. (2011). "Sugarcane bagasse whiskers: Extraction and characterizations," *Ind. Crop. Prod.* 33(1), 63-66. DOI: 10.1016/j.indcrop.2010.08.009

De, S. K., and White, J. R. (1996). *Short Fibre-polymer Composites*, Woodhead Publishing, Cambridge, United Kingdom.

Fahma, F., Iwamoto, S., Hori, N., Iwata, T., and Takemura, A. (2010). "Isolation, preparation, and characterization of nanofibers from oil palm empty-fruit-bunch (OPEFB)," *Cellulose* 17, 977-985. DOI: 10.1007/s10570-010-9436-4

Fortunati, E., Armentano, I., Iannoni, A., Barbale, M., Zaccheo, S., Scavone, M., Visai, L, and Kenny, J. M. (2012). "New multifunctional poly (lactide acid) composites: Mechanical, antibacterial, and degradation properties," *J. Appl. Polym. Sci.* 124(1), 87-98. DOI: 10.1002/app.35039

Fortunati, E., Puglia, D., Monti, M., Santulli, C., Maniruzzaman, M., and Kenny, J. M. (2013). "Cellulose nanocrystals extracted from okra fibers in PVA nanocomposites," *J. Appl. Polym. Sci.* 128(5), 3220-3230. DOI: 10.1002/app.38524

Frone, A. N., Berlioz, S., Chailan, J. F., Panaitescu, D. M., and Donescu, D. (2011). "Cellulose fiber-reinforced polylactic acid," *Polym. Composite.* 32(6), 976-985. DOI: 10.1002/pc.21116

Fu, S.-Y., Feng, X.-Q., Lauke, B., and Mai, Y.-W. (2008). "Effects of particle size, particle/matrix interface adhesion and particle loading on mechanical properties of particulate–polymer composites," *Compos. Part B-Eng.* 39(6), 933-961. DOI: 10.1016/j.compositesb.2008.01.002

Hernández, J. A., Romero, V. H., Escalante, A., Toriz, G., Rojas, O. J., and Sulbarán, B. C. (2018). "*Agave tequilana* bagasse as source of cellulose nanocrystals via organosolv treatment," *BioResources* 13(2), 3603-3614.

Hossain, K. M. Z., Ahmed, I., Parsons, A. J., Scotchford, C. A., Walker, G. S., Thielemans, W., and Rudd, C. D. (2012). "Physico-chemical and mechanical properties of nanocomposites prepared using cellulose nanowhiskers and poly(lactic acid)," *J. Mater. Sci.* 47, 2675-2686. DOI: 10.1007/s10853-011-6093-4

Indarti, E., Roslan, R., Husin, M., and Daud, W. R. W. (2016). "Polylactic acid bionanocomposites filled with nanocrystalline cellulose from TEMPO-oxidized oil palm lignocellulosic biomass," *BioResources* 11(4), 8615-8626. DOI: 10.15376/biores.11.4.8615-8626

Ismail, H., Jaffri, R. M., and Rozman, H. D. (2003). "The effects of filler loading and vulcanization system on properties of oil palm wood flour-natural rubber composites," *J. Elastom. Plast.* 35(2), 181-192. DOI: 10.1177/0095244303035002006

Jaratrotkamjorn, R., Khaokong, C., and Tanrattanakul, V. (2012). "Toughness enhancement of poly(lactic acid) by melt blending with natural rubber," *J. Appl. Polym. Sci.* 124(6), 5027-5036. DOI: 10.1002/app.35617

Johar, N., Ahmad, I., and Dufresne, A. (2012). "Extraction, preparation and characterization of cellulose fibres and nanocrystals from rice husk," *Ind. Crop. Prod.* 371(1), 93-99. DOI: 10.1016/j.indcrop.2011.12.016

Kargarzadeh, H., Ahmad, I., Abdullah, I., Dufresne, A., Zainudin, S. Y., and Sheltami, R. M. (2012). "Effects of hydrolysis conditions on the morphology, crystallinity, and thermal stability of cellulose nanocrystals extracted from kenaf bast fibers," *Cellulose* 19(3), 855-866. DOI: 10.1007/s10570-012-9684-6

Kargarzadeh, H., Johar, N., and Ahmad, I. (2017). "Starch biocomposite film reinforced by multiscale rice husk fiber," *Compos. Sci. Technol.* 151, 147-155. DOI: 10.1016/j.compscitech.2017.08.018

Kassab, Z., Aziz, F., Hannache, H., Youcef, H. B., and El Achaby, M. (2019). "Improved mechanical properties of *k*-carrageenan-based nanocomposite films reinforced with cellulose nanocrystals," *Int. J. Biol. Macromol.* 123, 1248-1256. DOI: 10.1016/j.ijbiomac.2018.12.030

Khoshkava, V., and Kamal, M. R. (2014). "Effect of cellulose nanocrystals (CNC) particle morphology on dispersion and rheological and mechanical properties of polypropylene/CNC nanocomposites," *ACS Appl. Mater. Inter.* 6(11), 8146-8157. DOI: 10.1021/am500577e

Liu, C., Li, B., Du, H., Lv, D., Zhang, Y., Yu, G., Mu, X, and Peng, H. (2016). "Properties of nanocellulose isolated from corncob residue using sulfuric acid, formic acid, oxidative and mechanical methods," *Carbohyd. Polym.* 151, 716-724. DOI: 10.1016/j.carbpol.2016.06.025

Lizundia, E., Vilas, J. L., and León, L. M. (2015). "Crystallization, structural relaxation and thermal degradation in poly(L-lactide)/cellulose nanocrystal renewable nanocomposites," *Carbohyd. Polym.* 123, 256-265. DOI: 10.1016/j.carbpol.2015.01.054

Mariano, M., El Kissi, N., and Dufresne, A. (2016). "Cellulose nanocrystal reinforced oxidized natural rubber nanocomposites," *Carbohyd. Polym.* 137, 174-183. DOI: 10.1016/j.carbpol.2015.10.027

Mathew, V. S., Sinturel, C., George, S. C., and Thomas, S. (2010). "Epoxy resin/liquid natural rubber system: Secondary phase separation and its impact on mechanical properties," *J. Mater. Sci.* 45(7), 1769-1781. DOI: 10.1007/s10853-009-4154-8

Ock, H. G., Kim, D. H., Ahn, K. H., Lee, S. J., and Maia, J. M. (2016). "Effect of organoclay as a compatibilizer in poly(lactic acid) and natural rubber blends," *Eur. Polym. J.* 76, 216-227. DOI: 10.1016/j.eurpolymj.2016.01.042

Pongsathit, S., and Pattamaprom, C. (2018). "Irradiation grafting of natural rubber latex with maleic anhydride and its compatibilization of poly(lactic acid)/natural rubber blends," *Radiat. Phys. Chem.* 144, 13-20. DOI: 10.1016/j.radphyschem.2017.11.006

Roman, M., and Winter, W. T. (2004). "Effect of sulfate groups from sulfuric acid hydrolysis on the thermal degradation behavior of bacterial cellulose," *Biomacromolecules* 5(5), 1671-1677. DOI: 10.1021/bm034519+

Rosli, N. A., Ahmad, I., and Abdullah, I. (2013). "Isolation and characterization of cellulose nanocrystals from *Agave angustifolia* fibre," *BioResources* 8(2), 1893-1908. DOI: 10.15376/biores.8.2.1893-1908

Rosli, N. A., Ahmad, I., Anuar, F. H., and Abdullah, I. (2016). "Mechanical and thermal properties of natural rubber-modified poly(lactic acid) compatibilized with telechelic liquid natural rubber," *Polym. Test.* 54, 196-202. DOI: 10.1016/j.polymertesting.2016.07.021

Rosli, N. A., Ahmad, I., Anuar, F. H., and Abdullah, I. (2018). "The contribution of eco-friendly bio-based blends on enhancing the thermal stability and biodegradability of poly(lactic acid)," *J. Clean. Prod.* 198, 987-995. DOI: 10.1016/j.jclepro.2018.07.119

Rosli, N. A., Ahmad, I., Anuar, F. H., and Abdullah, I. (2019a). "Effectiveness of cellulosic *Agave angustifolia* fibres on the performance of compatibilized poly(lactic acid)-natural rubber blends," *Cellulose* 26(5), 3205-3218. DOI: 10.1007/s10570-019-02262-x

Rosli, N. A., Ahmad, I., Anuar, F. H., and Abdullah, I. (2019b). "Application of polymethylmethacrylate-grafted cellulose as reinforcement for compatibilized polylactic acid/natural rubber blends," *Carbohyd. Polym.* 213, 50-58. DOI: 10.1016/j.carbpol.2019.02.074

Samir, M. A. S. A., Alloin, F., Sanchez, J.-Y., and Dufresne, A. (2004). "Cellulose nanocrystals reinforced poly(oxyethylene)," *Polymer* 45(12), 4149-4157. DOI: 10.1016/j.polymer.2004.03.094

Shah, B. L., Selke, S. E., Walters, M. B., and Heiden, P. A. (2008). "Effects of wood flour and chitosan on mechanical, chemical, and thermal properties of polylactide," *Polym. Compos.* 29(6), 655-663. DOI: 10.1002/pc.20415

Sheltami, R. M., Abdullah, I., Ahmad, I., Dufresne, A., and Kargarzadeh, H. (2012). "Extraction of cellulose nanocrystals from mengkuang leaves (*Pandanus tectorius*)," *Carbohyd. Polym.* 88(2), 772-779. DOI: 10.1016/j.carbpol.2012.01.062

Si, W.-J., Yuan, W.-Q., Li, Y.-D., Chen, Y.-K., and Zeng, J.-B. (2018). "Tailoring toughness of fully biobased poly(lactic acid)/natural rubber blends through dynamic vulcanization," *Polym. Test.* 65, 249-255. DOI: 10.1016/j.polymertesting.2017.11.030

Thomas, M. G., Abraham, E., Jyotishkumar, P., Maria, H. J., Pothen, L. A., and Thomas, S. (2015). "Nanocelluloses from jute fibers and their nanocomposites with natural rubber: Preparation and characterization," *Int. J. Biol. Macromol.* 81, 768-777. DOI: 10.1016/j.ijbiomac.2015.08.053

Trache, D., Hussin, M. H., Haafiz, M. K. M., and Thakur, V. K. (2017). "Recent progress in cellulose nanocrystals: Sources and production," *Nano-scale* 9(5), 1763-1786. DOI: 10.1039/C6NR09494E

Tronc, E., Hernández-Escobar, C. A., Ibarra-Gómez, R., Estrada-Monje, A., Navarrete-Bolaños, J., and Zaragoza-Contreras, E. A. (2007). "Blue agave fiber esterification for the reinforcement of thermoplastic composites," *Carbohyd. Polym.* 67(2), 245-255. DOI: 10.1016/j.carbpol.2006.05.027

Visakh, P.M., Thomas, S., Oksman, K., and Mathew, A.P. (2012). "Effect of cellulose nanofibers isolated from bamboo pulp residue on vulcanized natural rubber," *BioResources*, 7(2), 2156-2168.

Wan Ishak, W. H., Rosli, N. A., and Ahmad, I. (2020). "Influence of amorphous cellulose on mechanical, thermal, and hydrolytic degradation of poly (lactic acid) biocomposites," *Sci. Rep.* 10(1), 1-13. DOI: https://doi.org/10.1038/s41598-020-68274-x

Zainuddin, N., Ahmad, I., Kargarzadeh, H., and Ramli, S. (2017). "Hydrophobic kenaf nanocrystalline cellulose for the binding of curcumin," *Carbohyd. Polym.* 163, 261-269. DOI: 10.1016/j.carbpol.2017.01.036

Zhang, C., Huang, Y., Luo, C., Jiang, L., and Dan, Y. (2013). "Enhanced ductility of polylactide materials: Reactive blending with pre-hot sheared natural rubber," *J. Polym. Res.* 20(4), 1-9. DOI: 10.1007/s10965-013-0121-9

Article submitted: April 7, 2020; Peer review completed: June 13, 2020; Revised version received and accepted: May 13, 2021; Published: June 16, 2021.
DOI: 10.15376/biores.16.3.5538-5555